RSC Advances

PAPER

View Article Online
View Journal | View Issue

Cite this: *RSC Adv.*, 2026, **16**, 21601

Valorization of tannery fleshing waste into high energy biofuel through pyrolysis: process optimization and fuel properties analysis

Mohammad Al Shahriar Khan, [a] Manjushree Chowdhury,[a] Masud Hassan [b] and Amal Kanti Deb *[a]

Fleshing waste (FW) is an unavoidable solid waste generated during the fleshing operation of the leather tanning process. FW is hazardous because it contains significant amounts of sulfides and harms the environment by polluting soil and water, and emits greenhouse gases. This study examined the pyrolysis process for producing biofuel from FW and optimized the process parameters using response surface methodology. FW contains 3.77% moisture, 15.68% ash, 71.24% volatile matter, and 9.31% fixed carbon based on dry mass, according to proximate analysis. Ultimate analysis determined 50.41% C, 9.79% H, 4.02% N, 0.24% S, and 19.85% O in FW by dry mass, yielding a higher heating value of 27.62 MJ kg^{-1} and a lower heating value of 25.48 MJ kg^{-1}. Under optimized conditions (555 °C, 60 minutes, and 1 L h^{-1} N_2 flow rate), the pyrolysis process yielded 55% biofuel from FW. FTIR analysis of biofuel identified absorption bands at 3350, 2920, 2855, 1660, and 1455 cm^{-1} corresponding to –OH and –NH stretching, –CH stretching, –C=O stretching, and –CH bending groups. The biofuel exhibits enhanced energy density and ease of handling, with a calorific value of 40.24 MJ kg^{-1}, a kinematic viscosity of 2.12 cSt, and a density of 860 kg m^{-3}. Chemical stability of the biofuel is ensured by an acid value of 16 mg KOH per g. Fuel safety is ensured by a flash point of 60 °C and a fire point of 78 °C. GC-MS analysis of biofuel detected significant compounds like decahydro-8*a*-ethyl-1,1,4*a*,6-tetramethylnaphthalene and 1-methyl-2-propylpyrazolium bromide along with other active components. Therefore, the produced biofuel offers practical application potential, promotes sustainable waste management in the leather industry, and creates opportunities for a renewable energy source.

Received 31st December 2025
Accepted 16th April 2026

DOI: 10.1039/d5ra10133f

rsc.li/rsc-advances

1. Introduction

The leather tanning sector has a long history and is essential to the demands of society and the world economy. Animal hides and skins are tanned to make leather, but this process generates significant waste. When one ton of hide is processed, only 200 kg of leather is produced, along with 600 kg of tanned and non-tanned solid waste, and 200 kg of dissolved residue appears in wastewater.[1] Every year, the leather processing sector produces over 6 million tons of solid waste globally, of which 50–60% is fleshing waste (FW).[2] FW is generated during the fleshing operation of hides and skins (pelts) after the liming-unhairing process, and usually contains 4–18% fat, 5–7% protein, 2–6% lime, and 2–4% sulfide on a wet-mass basis.[3] Additionally, FW contains sodium sulfide, a caustic and toxic substance that poses environmental risk.[4] The high concentration of toxic water from FW pollutes the soil, surface water, and groundwater substantially. When FW comes into contact with acidic substances and the pH drops to 8.5 or lower, a high concentration of H_2S gas is produced, causing severe health hazards and air pollution.[5] In addition, when the protein and fatty substances in FW decompose, it produces greenhouse gases (GHGs), primarily methane. At present, FW is generally not recycled and instead ends up in landfills or is dumped in open areas, which can lead to soil contamination, increase alkalinity, and leave toxic residues. Rainwater transports hazardous constituents from fleshing waste into nearby water bodies, posing serious risks to aquatic ecosystems and humans.

Several approaches to valorize FW have been reported in the literature to overcome ecological and economic pitfalls associated with it. These include anaerobic digestion for biogas production,[6] bacterial composting,[7] biodiesel production *via* transesterification,[8] and hydrolysate production.[9] Although these methods have advantages, there are also shortcomings, such as low efficiency, the generation of toxic by-products, secondary pollution, high operating costs, and complex procedures. To address these challenges, the pyrolysis process is proposed in this study as an alternative to conventional recovery

[a]*Institute of Leather Engineering and Technology, University of Dhaka, Dhaka-1000, Bangladesh. E-mail: debak.ilet@du.ac.bd*

[b]*College of Resources and Environmental Engineering, Guizhou University, Guiyang, Guizhou 550025, China*

methods to reduce the environmental impact and financial costs associated with leather solid waste.

Pyrolysis involves heating carbonaceous materials within an inert atmosphere, transforming them into gases, oils, and carbonaceous residue (biochar) at high temperatures.[10] Pyrolysis is superior to combustion because it produces fewer greenhouse gas emissions that contribute to global warming. The results of pyrolysis depend on various parameters, including biomass composition, temperature, residence time, carrier gas flow rate, heating rate, and particle size.[11] Various biomasses have been employed for pyrolysis over the years. Shadangi *et al.*, 2014 pyrolyzed Karanja seeds in a semi-batch reactor at 550 °C, and the highest biofuel obtained was 55.2%.[12] The pyrolysis of Mediterranean seaweed (*Posidonia oceanica*) generated biofuel yield of 52.4% with 32% biochar at 400 °C, and white pine produced 47.4% biofuel at 500 °C and 26.4% biochar at 400 °C.[13] A microwave-based pyrolysis of lignocellulosic feedstock such as bamboo leaves, rice husks, corn stalks, sugarcane bagasse, sugarcane peel trash, coffee ash, and paddy straw was carried out with biochar yields between 18–22%, biofuel yields between 40–48%, and syngas of 30–40%.[14] Tallow (animal fat) was thermally decomposed by pyrolysis in a fixed-bed reactor at laboratory scale, with a highest 12.47% biofuel yield obtained in optimum conditions of 350 °C and 140 minutes.[15] The pyrolysis of chrome shaving dust from tannery waste yielded 49% biofuel, 21% syngas, and 30% biochar, whereas leather finished trimmings produced 52% biofuel, 21% syngas, and 27% biochar in a fixed-bed pyrolysis unit.[16] However, the heavy metals, including chromium, lead, and cadmium, in the solid residue from the pyrolysis of tanned and finished solid leather wastes limit their practical application. On the other hand, research on non-tanned leather solid waste, such as FW, is scarce, and it contains no heavy metals; the char after pyrolysis can be safely utilized. Therefore, the current study attempts to fill this gap by considering the pyrolysis of tannery FW to produce high-energy content biofuel.

At present, fossil fuels have extremely high global demand owing to their dominant use in both the industrial and transportation sectors.[17] The burning of fossil fuels results in pollutants, including unburned hydrocarbons, nitrogen oxides, carbon dioxide, and volatile organic compounds. The GHGs exacerbate climate change, the implications of which (warmer temperature) is a serious threat to humanity around the world.[18] As a result, researchers, development practitioners, and industrialists are working hard to develop sustainable and viable solutions in the field of biofuels.[19] There is a global consensus on the advantages of using biofuel, such as green sourcing, low or no pollution, and affordability. In addition, biofuels reduce GHG emissions that cause global warming, reduce environmental pollution, and enhance the local economy.[20] FW pyrolysis to biofuel may have the potential to be an alternative to fossil fuels, as it may produce heat, electricity, and other value added products.

Although biofuel combustion results in fewer CO_2 emissions, it does not completely eliminate GHG emissions. The main objective of this study is to demonstrate a waste-to-energy valorization pathway for tannery fleshing waste. This approach can reduce environmental impacts by avoiding methane (CH_4) emissions from conventional FW disposal methods, such as landfilling. According to the Intergovernmental Panel on Climate Change (IPCC) Fifth Assessment Report (AR5), CH_4 has 28 times the 100-year global warming potential (GWP) of CO_2.[21] Additionally, the biofuel produced has the potential to replace fossil fuels partially, thereby reducing net carbon emissions.

The overarching goal of this work is to provide a sustainable solution for tannery FW through resource recovery, *i.e.*, biofuel production. The primary objectives are to pyrolyze FW to biofuel, determine the ideal operational conditions for maximum biofuel yield, examine the influence of key parameters including temperature, holding time, and N_2 flow rate on biofuel production, and conduct a comprehensive characterization of the synthesized biofuel.

2. Materials and methods

2.1 Raw materials

Fleshing waste (FW) was collected from Arafat Tannery, located at the tannery industrial estate in Savar, Dhaka (TIED), Bangladesh. The samples were taken during the fleshing operation of cow limed pelts after the liming-unhairing process. After washing several times, FW was delimed using ammonium chloride and ammonium sulfate to remove lime and sulfides. Afterward, the samples were allowed to air-dry for 7 days to reduce moisture content to less than 5% and were subsequently stored in glassware for future analytical assessment and experiments.

2.2 Raw material characterization

2.2.1 Proximate and ultimate analyses. The proximate analysis of pre-dried FW was determined using standard methods – ASTM E1756 for moisture level,[22] ASTM E1755-01 for ash (inorganic) fraction,[23] and ASTM E872-82 for volatile matter percentage.[24] Fixed carbon (FC) percentage was determined using FC = DM − (VM + Ash), where DM is the dry matter content (%), VM is the volatile matter content (%), and Ash is the ash content (%).

For elemental analysis, the pre-dried FW was analyzed using ASTM standard methods E777, E775, and E778 to determine carbon, hydrogen, nitrogen, and sulfur content with a CHNS analyzer (Vario MICRO Cube, Germany).[25] The oxygen (O) level was determined by subtracting the combined percentages of hydrogen, nitrogen, sulfur, carbon, and ash from 100%. About 3 mg of the sample was transferred to a tin capsule and then introduced into the automatic elemental analyzer. During the analysis, the combustion and reduction temperatures were 1150 °C and 850 °C, respectively, while the gases used for conveying were helium and oxygen. The higher and lower heating values (HHV and LHV) of the sample were determined using the Dulong equations, as depicted in SI eqn (S1) and (S2) (SI text I).[26,27]

2.2.2 Fourier transform infrared spectroscopy. Functional groups were characterized by using Fourier transform infrared spectroscopy (FTIR). Spectra were obtained at a resolution of 2 cm^{-1} for 64 scans using a FTIR spectrometer (ALPHA II, Germany). The solid samples were ground and then

compressed with KBr (1 : 100 by mass) into transparent pellets. After preparation, each specimen was placed into the spectrometer's sample holder, and absorption data were collected over the 400–4000 cm^{-1} wavenumber range. The observed spectra were analyzed to identify the functional groups present in the sample.[28]

2.2.3 Thermogravimetric and derivative thermogravimetric analysis. In the thermogravimetric analysis (TGA), the 8000™ (USA) TGA analyzer was used to monitor changes in the sample's mass as temperature varied under a maintained atmosphere. About 5–6 mg of the specimen was placed in a ceramic pan, and nitrogen gas (99.99% purity) at a flow rate of 20 mL min^{-1} was maintained in the system. The samples were subjected to a controlled heating rate of 10 °C min^{-1}, and the analysis was carried out within 50–800 °C. The thermal decomposition process was measured continuously using a TGA analyzer, providing insights into the sample's thermal characteristics.[29] To obtain the derivative thermogravimetric (DTG) curve, TGA data were numerically differentiated using the equation that estimates the weight-change rate as a function of temperature (SI eqn (S3), SI text I).

2.3 Pyrolysis experiment

The pyrolysis experiments were conducted in a small-scale fixed-bed reactor with an interior diameter of 15 cm and a height of 30 cm. The reactor was heated using an electric furnace. A photoionization detector was used to control the temperature accurately, and the K-type thermocouple in the middle was used to monitor it. The reactor was connected to a 200 mm-long steel condenser *via* a stainless-steel pipe, where the liquid condensate was collected. Water circulation was used to keep the condenser at a steady temperature of 25 °C. The experiment was performed under nitrogen gas flow at atmospheric pressure. Approximately 200 g of pre-dried FW was loaded onto the sample holder in the pyrolysis reactor, raised to a target temperature at various heating rates, and held at that temperature for specific durations.

2.4 Experimental design

Response surface methodology (RSM) with central composite design (CCD) was employed to optimize the pyrolysis process. CCD was chosen because it can model interaction and curvature with fewer experimental runs.[30] Temperature, holding time, and N_2 flow rate were chosen as key parameters. The total number of trials required was determined using the following equation.

$$N = 2^n + 2n + C_p = 2^3 + 2.3 + 3 = 17$$

where (n) and (C_p) are the number of variables and replicating central points, respectively.

However, three additional experiments were added to the original design to enhance the model's robustness and accuracy. The relationship between biofuel yield and influencing factors (temperature, time, and N_2 flow rate) can be expressed with the following second-order polynomial equation.

$$Y = \beta_o + \sum_{i=1}^{n} \beta_i \times X_i + \sum_{i=1}^{n} \beta_{ii} \times X_i^2 + \sum_{i=1}^{n} \sum_{j>1}^{n} \beta_{ij} \times X_i X_j$$

where Y is the anticipated result, n represents the complete set of experimental trials, X_i and X_j are experimental factors, and β_o, β_i, β_{ii}, and β_{ij} are the constant, linear, quadratic, and interaction coefficients, respectively.

Analysis of variance (ANOVA) was performed to assess how well the model fits the data. To better understand the influence of parameters, 3D response surface plots and 2D contour plots were generated to visualize the interactions among the variables. Optimization analysis, model validation, and graphical representation were all carried out using Design-Expert v25.0 software of Stat-Ease Inc.

2.5 Biofuel characterization

2.5.1 Fourier transform infrared spectroscopy. FTIR analysis of the biofuel was conducted under the same conditions as detailed in Section 2.2.2; however, the biofuel specimen was placed directly into the liquid sample holder of the instrument and captured FTIR spectra.

2.5.2 Fuel properties. A calibrated pycnometer was filled with biofuel and weighed to determine its density. The mass was then divided by the known volume at 25 °C, in accordance with ASTM D1217-12. Specific gravity was calculated using density by the formula stated in SI eqn (S4) (SI text I).

Biofuel's calorific value was assessed using the ASTM D240-19 standard test on a bomb calorimeter.[31] The biofuel sample was placed in a sealed combustion chamber (bomb) and filled with oxygen to ensure complete combustion. The bomb was submerged in a water bath with a known heat capacity, and the biofuel was ignited electrically. The heat produced during combustion increases the temperature of the surrounding water, and the energy content is derived from this temperature variation. Kinematic and dynamic viscosities were measured using a Saybolt Seconds Universal (SSU) viscometer in accordance with ASTM D445-24.[32] The SSU viscometer measured kinematic viscosity by measuring the flow time of 60 mL of fluid through a calibrated orifice under controlled temperature in an oil bath. The recorded SSU time was then converted to centistokes (Cst). The dynamic viscosity was subsequently calculated as the product of kinematic viscosity and liquid density.

The acid value of biofuel was determined by titration following the standard method of ASTM D664.[33] In that process, 2 g of the biofuel sample was refluxed with neutral ethanol and titrated with a standard potassium hydroxide (KOH) solution. Phenolphthalein was used as an indicator to determine the endpoint upon a pale pink color change. Acid value was determined by the equation as illustrated in SI eqn (S5) (SI text I).

A closed-cup standard method, as per ASTM D93, was employed to assess the flash and fire points of the biofuel.[34] This experiment used the Pensky-Martens Closed Cup Tester (Germany), in which the biofuel sample was enclosed in a sealed chamber and heated at a controlled rate. A small test flame was introduced at regular intervals to determine the minimum temperature at which vapors ignite (flash point). The

temperature at which the biofuel sustained combustion for at least 5 seconds was determined as the fire point. The biofuel's moisture and ash contents were measured under the same conditions as Section 2.2.1. A digital pH meter with a glass electrode was used to measure the biofuel's pH in accordance with ASTM E70-19.[35] The pH meter was standardized with buffer solutions before analyzing the pH of the biofuel sample.

2.5.3 Gas chromatography-mass spectrometry analysis. The gas chromatographic analysis was performed by using an Agilent 7890 (GC) and Agilent 5975 (MS), USA system. Biofuel was evaporated under nitrogen and mixed with toluene. Methylation was carried out using acetyl chloride in methanol under heat. After cooling, the reaction was quenched with purified water. Fatty acid methyl esters were extracted using a non-polar solvent mixture, isolated, and redissolved; components were identified using external standards and spectral databases. The whole GC-MS process was performed in accordance with Cavonius *et al.*, 2014.[36]

3. Results and discussion

3.1 Feed material characteristics

3.1.1 Physicochemical properties of fleshing waste. Table 1 summarizes the physicochemical characteristics of pre-dried FW. The studied FW has clear advantages over most other leather solid wastes because it has a moisture content of only 3.77 wt%. This is in sharp contrast to animal fleshing waste and chrome-tanned leather waste, which have reported moisture levels of 77.5 wt% and 36.9 wt%.[37,38] This low moisture content increases the FW's ability to undergo thermochemical pyrolysis, since excessive moisture can impede effectiveness. FW contains 15.68 wt% ash, compared to 5.25 wt% in leather waste and 51.5 wt% in animal raw fleshing waste. This shows that the inorganic content varies with how the hide pelt is processed during liming-unhairing operation.[37,39] FW has a high volatile matter of 71.24 wt%, making it exceptional in energy recovery. In contrast, the fixed carbon content of FW is moderate (9.31 wt%).

Table 1 The results of the proximate and ultimate analysis of FW

Characteristics	Fleshing waste (wt%)
Proximate analysis	
Moisture content	3.77%
Ash content	15.68%
Volatile matter	71.24%
Fixed carbon	9.31%
Ultimate analysis	
C	50.41%
H	9.79%
N	4.02%
S	0.24%
O	19.85%
H/C	2.33
O/C	0.30
HHV	27.62 MJ kg^{-1}
LHV	25.48 MJ kg^{-1}

The ultimate analysis of FW shows high carbon and hydrogen contents of 50.41 wt% and 9.79 wt%, respectively. FW contains very low sulfur content (0.24 wt%), enabling cleaner energy conversion than other wastes with higher sulfur content, including chrome-tanned leather waste (1.09 wt%) and finished leather waste (3.43 wt%).[38,40] Since the FW were pre-treated, delimed, and washed several times, most of the unreacted inorganic sulfides were removed from the FW. The HHV of 27.62 MJ kg^{-1} and LHV of 25.48 MJ kg^{-1} highlight the energy potential of the tannery FW, as these values are higher than those of chrome-tanned leather waste (12–14 MJ kg^{-1}) and other tannery wastes.[37–41]

3.1.2 Functional groups composition and thermal behavior of fleshing waste. The Fourier transform infrared spectroscopy (FTIR) of FW waste highlights its complex chemical composition with a wide range of functional groups in Fig. 1(A). The broad absorption band at approximately 3400 cm^{-1} relates to both –OH and –NH stretching vibrations, indicating hydroxyl groups from water and amide groups from protein.[42] Strong peaks at 2850 and 2916 cm^{-1} reflected the –CH stretching vibrations of alkanes.[43] An intense band at 1740 cm^{-1} indicates –C═O stretching vibrations that are generally assigned to the carbonyl groups.[44] Another peak at 1640 cm^{-1} is attributed to the amide I vibration of collagen. The sharp peak at 1539 cm^{-1} is attributed to amide II vibrations, confirming that the waste material was proteinaceous.[45] The absorption band at 1459 cm^{-1} corresponds to –CH bending vibration of alkanes, and signals at around 1175 and 1104 cm^{-1} can be ascribed to –CO stretching, indicating the presence of esters or ethers.[46] The peak observed at 720 cm^{-1} in the low-wavenumber region is due to the rocking vibration of the methylene group (–CH_2–) and is characteristic of long-chain hydrocarbons.[47]

The thermogram analysis of pre-dried FW, obtained from thermogravimetric analysis (TGA) and derivative thermogravimetric (DTG) curves, is illustrated in Fig. 1(B), highlighting four distinct decomposition phases. The first weight-loss stage occured at approximately 100 °C and was attributed to the gradual volatilization of moisture present in the sample. This was followed by an exothermic peak at 325 °C, corresponding to the decomposition of fatty substances. This stage was characterized by the maximum decomposition rate of −0.47% $°C^{-1}$ and a total mass loss of 39.11%. The third stage, with a peak at 460 °C, indicateed the degradation of proteinaceous material, with a peak decomposition rate of −0.24% $°C^{-1}$ and an additional weight loss of 18.79%. The last decomposition stage occured at approximately 700 °C, indicating the complete breakdown of FW, and contributed 7.0% mass loss at a maximum rate of −0.12% $°C^{-1}$. Overall, the TGA and DTG analyses provide insights into the active pyrolysis zone, which falls between 325 °C and 700 °C.

3.2 Statistical modeling and process optimization of biofuel yield

3.2.1 Design of experiments and statistical evaluation. This study investigated the association between the response (biofuel yield) and three input variables (temperature, time, and

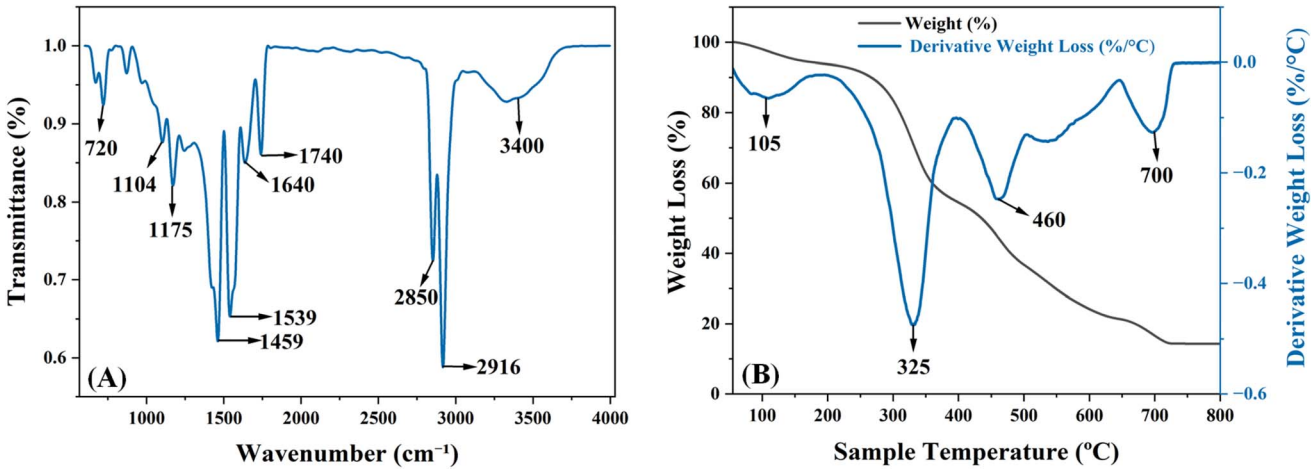

Fig. 1 (A) FTIR spectra of FW showing the different functional groups, (B) TGA and DTG curves exhibiting various thermal phase decomposition of FW.

nitrogen flow rate) in the pyrolysis of FW. Table 2 depicts the experimental outcomes of biofuel production within the defined parameter range, as recommended by the Central Composite Design (CCD). The following polynomial-coded equation depicts the association among the variables for forecasting biofuel yield.

$$\text{Biofuel} = 46.91 + 0.39A + 0.65B - 6.23C + 0.823AB - 2.74AC + 4.05BC - 14.70A^2 - 4.89B^2 + 2.00C^2$$

where A, B, and C represent the encoded labels for the three chosen variables: A: temperature, B: time, and C: nitrogen flow rate. The sign of each coefficient reveals interaction behavior: positive for synergy, negative for antagonism.

The evaluation of various regression models such as Linear, 2FI (Two-Factor Interaction), Quadratic, and Cubic to identify the most suitable match for this experimental dataset is presented in Table S1. Among these, the Quadratic model is the most appropriate, with a highly significant sequential p-value (<0.0001), an adequate p-value (0.0647), a high adjusted R^2 (0.9664), and a predicted R^2 (0.8077). These values imply that the model can interpret and predict the data's variance. The Quadratic model's strong fit is also supported by its statistical measures; a low standard deviation (1.89) and high R^2 (0.9823) indicate minimal variation and excellent correlation with the data. The adequate precision value of 29.4692 is considerably larger than the minimum threshold of 4, indicating an excellent signal-to-noise ratio.

Table 2 CCD of independent variables (temperature, time, and nitrogen flow rate) for optimizing process parameters and evaluating their combined effects on biofuel production

Run	A: Temperature (°C)	B: Time (min)	C: N_2 flow rate (L h^{-1})	Response biofuel (%)
1	400	90	5	30
2	550	60	3	47
3	400	60	3	33
4	700	30	5	15
5	550	60	5	45
6	600	60	1	54.5
7	550	60	3	47
8	550	90	3	42
9	400	90	1	28
10	700	30	1	40
11	550	60	3	45
12	400	30	5	20
13	400	30	1	38
14	600	90	1	48
15	700	60	3	35
16	700	90	5	25
17	550	30	3	43
18	400	60	1	36
19	550	60	3	46
20	550	60	3	45

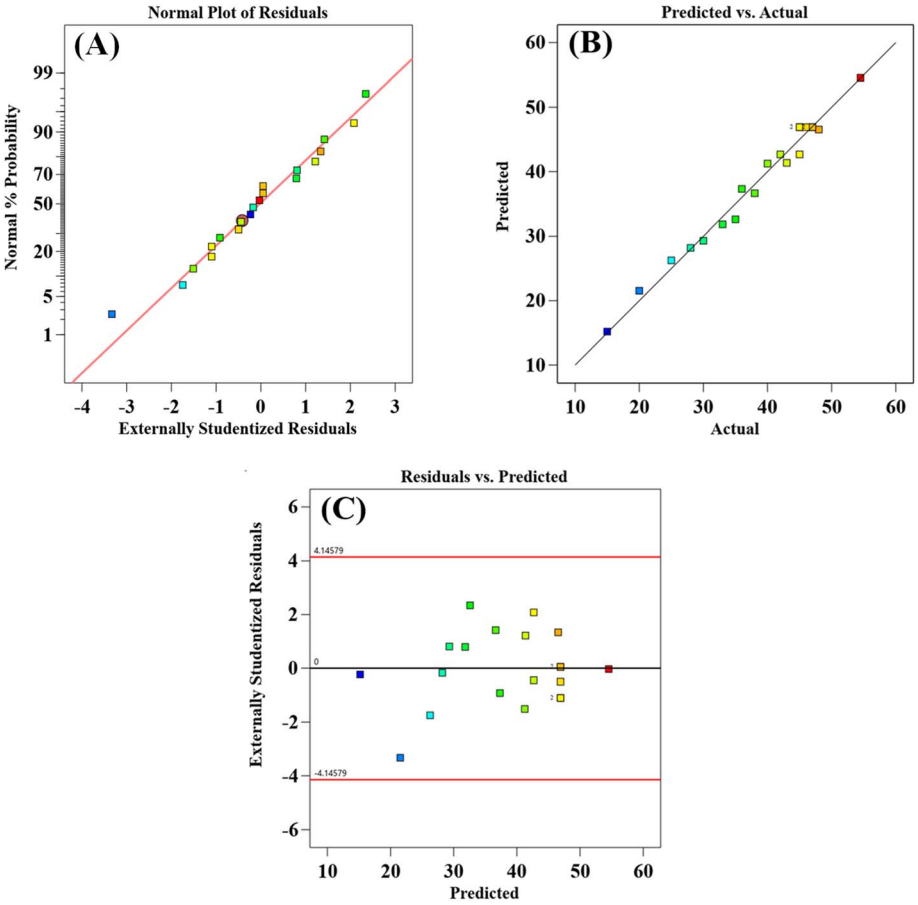

Fig. 2 Diagnostic plots for the Quadratic model validation: (A) normal probability plot of residuals, (B) predicted *versus* actual response values, and (C) residuals *versus* predicted values.

Moreover, the Quadratic model is also validated by the diagnostic plots in Fig. 2. The Fig. 2(A) shows that externally studentized residuals align closely with the expected normal distribution, which confirms the normality of the residuals. The predicted *vs.* actual plot in Fig. 2(B) shows that the linear relationship is strong, implying high predictive accuracy. The residuals *vs.* predicted plot in Fig. 2(C) reveals random scatter within the standard control limits, supporting homoscedasticity and model stability. Collectively, these diagnostics confirm that the Quadratic model has good statistical integrity and reliability in representing the data structure in this study.

Table 3 also demonstrates that the overall Quadratic model is statistically significant (F-value = 61.64, and p-value < 0.0001). Among the individual factors, nitrogen flow rate has a significant impact (p-value < 0.0001), whereas temperature and time alone are not significant (p-values of 0.5506 and 0.3137, respectively). Interaction terms, such as *AC* (temperature × N_2 flow rate) and *BC* (time × N_2 flow rate), as well as quadratic terms like A^2, B^2, and C^2, are also significant. This means there is a non-linear association and interaction between the variables. The insignificant lack-of-fit (p-value = 0.0647), low residual variance (35.66), and significant contribution of key terms demonstrate that this model is robust and offers a valuable contribution to the study of the pyrolysis process.

3.2.2 Process parameter interactions on biofuel yield. The 3D visualizations of various interactions, such as temperature and time, temperature and N_2 flow rate, and time and N_2 flow rate, are presented in Fig. 3(A), 4(A), 5(A) and 2d contour plots are presented in Fig. 3(B), 4(B) and 5(B).

The effect of temperature and time on biofuel yield was examined at a constant N_2 flow rate of 3 L h^{-1}, as shown in Fig. 3. The analysis revealed that, as temperature increased, biofuel yield initially rose to a maximum before declining as temperature rose further. This is probably due to increased formation of volatiles (H_2, CH_4, and CO) at higher temperatures.[48] Also, beyond critical temperature, exposure to higher temperature speeds up crosslinking and repolymerization, resulting in enhanced biochar and syngas production rather than biofuel.[49] These results are consistent with the ANOVA analysis, which indicated that the quadratic term for temperature (temperature^2) was significant, whereas the linear term for temperature was not. This nonlinear effect is statistically significant (F-statistic = 162.39 and p-value < 0.0001 for the quadratic term). Time also showed a similar nonlinear trend in its effect on biofuel yield, although it was smaller than that observed for temperature (F-value of 23.51 and p-value of 0.0007 for the quadratic term). However, the interaction of time and

Table 3 Statistical significance analysis of the Quadratic model and model terms based on ANOVA for evaluating the influence of temperature, time, and nitrogen flow rate on biofuel production

Source	Sum of squares	Degree of freedom	Mean square	*F*-Value	*p*-Value	Remarks
Model	1978.28	9	219.81	61.64	<0.0001	Significant
A-Temperature	1.36	1	1.36	0.3816	0.5506	
B-Time	4.01	1	4.01	1.13	0.3137	
C-N_2 flow rate	392.69	1	392.69	110.13	<0.0001	Significant
AB	4.30	1	4.30	1.21	0.2979	
AC	52.62	1	52.62	14.76	0.0033	Significant
BC	120.45	1	120.45	33.78	0.0002	Significant
A^2	579.07	1	579.07	162.39	<0.0001	Significant
B^2	83.82	1	83.82	23.51	0.0007	Significant
C^2	11.87	1	11.87	3.33	0.0980	Significant
Residual	35.66	10	3.57			
Lack of fit	31.66	6	5.28	5.28	0.0647	Not significant
Pure error	4.00	4	1.00			
Cor. total	2013.94	19				

temperature (*AB*) was not statistically significant with a *p*-value of 0.2979.

Subsequently, a further evaluation was performed to examine the interaction of temperature and N_2 flow rate with the reaction time fixed at 60 minutes (Fig. 4). The findings showed that biofuel yield increased up to the optimum temperature, and further temperature increases induced secondary cracking of volatiles, thereby reducing yield (consistent with previous findings). In comparison, the impact of N_2 flow rate on biofuel yield was inversely linear: higher N_2 flow rates reduced biofuel production. The decrease was due to the reduced residence time of the volatile compounds in the pyrolysis reactor, which prevented them from condensing and producing biofuel.[50] ANOVA analysis demonstrated that N_2 flow rate had a highly significant effect on biofuel yield ($F = 110.13$, $p < 0.0001$). In addition, the interaction term between temperature and N_2 flow rate (*AC*) is significant ($F = 14.76$, $p = 0.0033$).

Finally, the impact of time and N_2 flow rate on biofuel yield was explored by keeping the temperature constant at 550 °C (Fig. 5). It was found that time had a parabolic effect on biofuel yield, and N_2 flow rate had an inverse effect (consistent with previous findings). Statistical analysis confirmed the significance of the quadratic term for time and the linear term for N_2 flow rate. The interaction of time and N_2 flow rate (*BC*) was also statistically significant with an *F*-value of 33.78 and a *p*-value of 0.0002.

3.2.3 The optimal reaction conditions. The analysis of data from 20 experiments using Design-Expert software revealed that the optimum reaction conditions for maximizing biofuel yield were 558 °C, 63 minutes, and a 1 L h^{-1} N_2 flow rate; however, slight adjustments were made during actual experiments due to equipment limitations. The applied conditions were 555 °C, 60 minutes, and 1 L h^{-1} N_2 flow rate.

Three experimental validation tests were performed using these optimum conditions, and the average biofuel yield was obtained to be 55.10%, which is consistent with the predicted value (Table 4). This yield is comparable to that of biofuel produced from other feedstocks. However, the quality of fuel produced in this case appears superior, as evaluated in Section 3.3 of the biofuel property section. This enhancement is due to

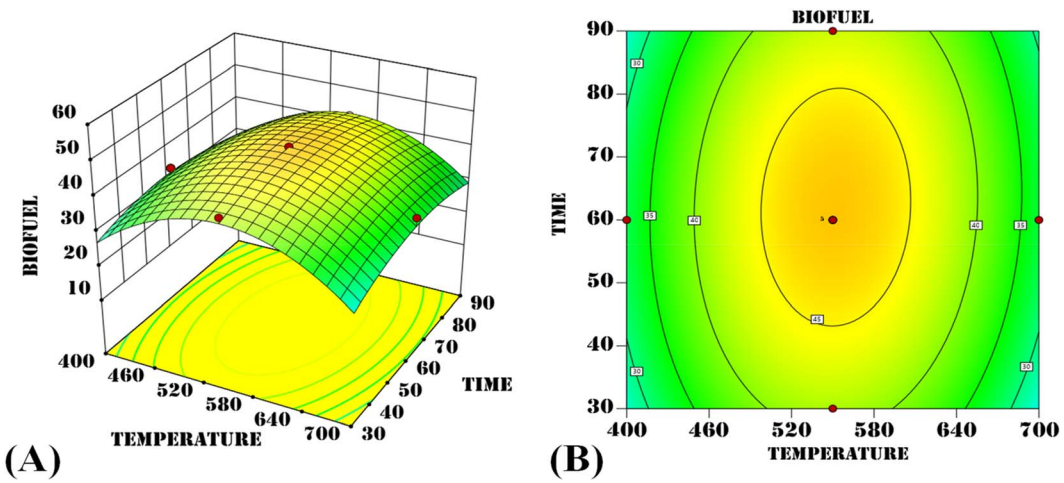

Fig. 3 (A) 3D surface plot, and (B) 2D contour plot depicting the combined influence of temperature and time on biofuel yield.

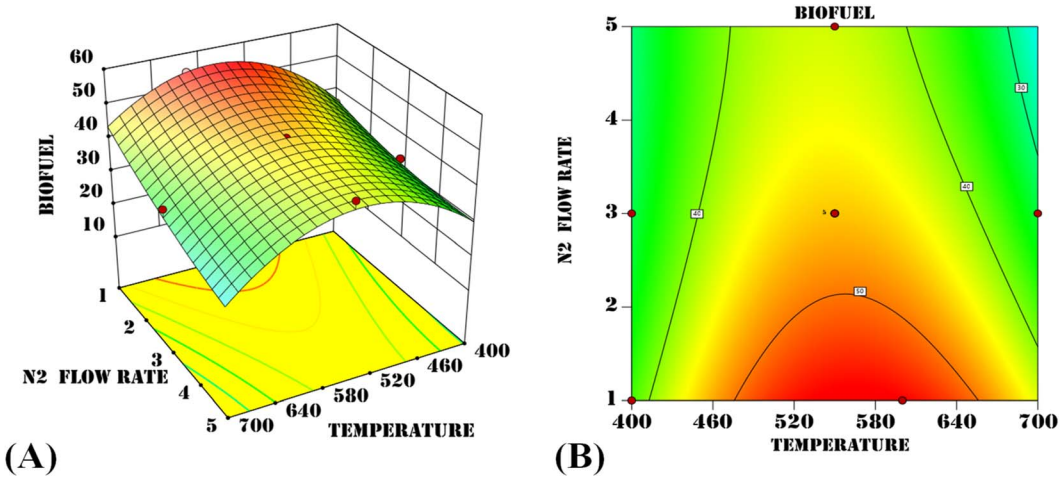

Fig. 4 (A) 3D surface plot, and (B) 2D contour plot illustrating the combined influence of temperature and N_2 flow rate on biofuel yield.

the composition of fleshing waste, which is especially high in protein and fat.

3.3 Biofuel properties

3.3.1 Biofuel functional group composition. As shown in Fig. 6(A), a broad absorption band near 3350 cm^{-1} is attributed to the stretching vibrations of –OH and –NH groups.[51] These stretching vibrations are associated with hydroxyl groups in water or alcohols, as well as with amines or amides in proteins. Strong bands near region 2855 and 2920 cm^{-1} represent –CH stretching vibrations and signify a higher alkane component in the sample.[52] Alkanes are important energy carriers due to their excellent combustion properties. The band detected at 1660 cm^{-1} is particularly significant because it corresponds to –C═O stretching vibrations, which are typically associated with conjugated carbonyl groups.[53,54] Furthermore, the presence of an absorption band at 1455 cm^{-1} indicates –CH bending vibrations in alkanes and highlights the biofuel's hydrocarbon structure.[55] At lower wavelengths, peaks at 1034 and 721 cm^{-1} that correspond to –C–O stretching and methylene ($–CH_2–$) rocking vibrations were observed.[46,47,56] These signals indicate a complex interaction between oxygenated and hydrocarbon components in the biofuel.

3.3.2 Fuel characterization and comparative evaluation of biofuel. The biofuel studied has excellent fuel properties and is a better energy source than other biofuels derived from switchgrass, wood, palm shells, and animal fat (Table 5). The ability of biofuel to meet, and sometimes exceed, ASTM Burner Fuel Standards demonstrates its potential as a highly efficient and eco-friendly fuel source. A key aspect of this biofuel is its calorific value of 40.24 MJ kg^{-1}, comparable to that of poultry fat biofuel at 40.32 MJ kg^{-1}.[57] This is much higher than the calorific values of biofuels from other sources, such as palm shell (26.93 MJ kg^{-1}), wood (23.10 MJ kg^{-1}), and switchgrass (18 MJ kg^{-1}).[58–60] Another important positive aspect of the synthesized biofuel is its viscosity, which helps during handling and operation. Its kinematic viscosity is 2.12 cSt at 40 °C, and the dynamic viscosity is 1.82 cP. The viscosity of the biofuel being

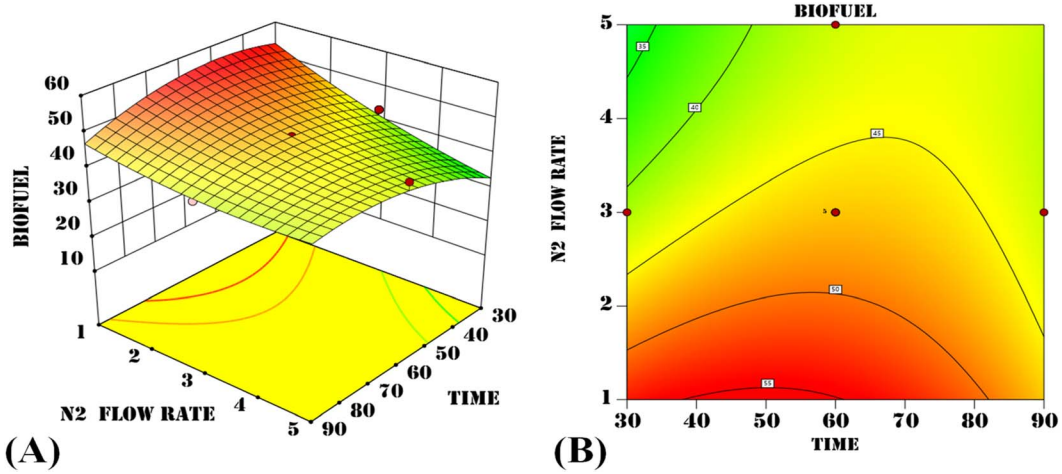

Fig. 5 (A) 3D surface plot, and (B) 2D contour plot showing the combined effect of time and N_2 flow rate on biofuel yield.

Table 4 Comparison of predicted and experimental biofuel yields under optimized process conditions of temperature, time, and nitrogen flow rate

	Temperature (°C)	Time (min)	N_2 flow rate (L h^{-1})	Biofuel yield (%)
Predicted	558	63	1	54.66
Experimental	555	60	1	55.10

investigated is significantly lower than that of the wood biofuel, whose kinematic viscosity is 134 cSt.[59] The biofuel also has a density of 860 kg m^{-3} and a specific gravity of 0.86. By comparison, palm shell pyrolysis biofuel has a greater density of 1110 kg m^{-3}, indicating that the examined biofuel is lighter and easier to handle.[60] This characteristic allows for improved transportation, storage, and integration into various applications. The acid value of the biofuel under investigation is 16 mg KOH per g, which is much less than that of animal fat (poultry) biofuel.[57] The low acidity leads to high chemical stability, minimizing the risk of corrosion during use and storage. This stability improves biofuels' overall compatibility and reliability with different handling conditions. Further, the biofuel produced has a flash point of 60 °C and a fire point of 78 °C. These values exceed the ASTM minimum specifications and demonstrate excellent safety characteristics for the biofuel's use, handling, and storage.[61]

The biofuel also has a very low ash content (0.01%) and a moderate alkaline pH of 8.5, which makes it less corrosive and harmful to the environment. Other pyrolysis biofuels are much more acidic, with a pH of 3.24 or lower.[57–60] Overall, the clean characteristics of the derived biofuel suggest it as a more eco-friendly and sustainable fuel alternative and further emphasize its effectiveness for use in industrial burners, engines, and power generation systems (Fig. S1 and S2). Besides, the cost of biofuel production from FW through the proposed method is significantly lower than that of conventional methods. The lab-scale production cost is only 0.33 USD L^{-1}, and this cost will be significantly lower at large-scale production (Table S2). In addition to biofuel, this system produces around 40% solid biochar, which is free of toxic chemicals, and suitable for environmental remediation, including soil and water treatment and carbon sequestration (Fig. S3). The remaining 5% is syngas, which can also be utilized as an energy source.

3.3.3 Gas chromatography-mass spectrometry analysis of biofuel. Biofuel is a highly complex blend comprising over 300 distinct hydrocarbon derivatives, including acids, alcohols, ketones, aldehydes, nitriles, esters, amines, and ethers.[62] Nanda *et al.*, 2014 also reported findings on monoaromatics, polyaromatics, aliphatics, oxygenates, and nitrogenates in biofuel from pyrolysis.[63] Analysis of the biofuel using gas chromatography-mass spectrometry (GC-MS) in this study also identified a range of hydrocarbons, oxygenates, and nitrogen-containing compounds (Fig. 6B and Table S3), which aligns with the FTIR result of the biofuel.

Among the identified compounds, decahydro-8*a*-ethyl-1,1,4*a*,6-tetramethylnaphthalene (M_W: 222, area: 11.57%) stands out for its significant contribution to the biofuel's energy density and combustion efficiency. Long-chain hydrocarbons, such as *z*-23-dotriaconten-2-one (M_W: 462, area: 3.06%), underscore the biofuel's potential as a high-energy fuel source. 1-methyl-2-propyl-pyrazolium bromide (M_W: 204, area: 10.40%) is another important component that affects fuel stability and ignition properties. Moreover, chemical compounds such as 2-pentadecanone (M_W: 226, area: 3.43%) and *n*-[4-cyclooctylaminobutyl] aziridine (M_W: 224, area: 3.58%) with the existing oxygen and nitrogen functional groups influence fuel stability, ignition performance, and emission remediation.

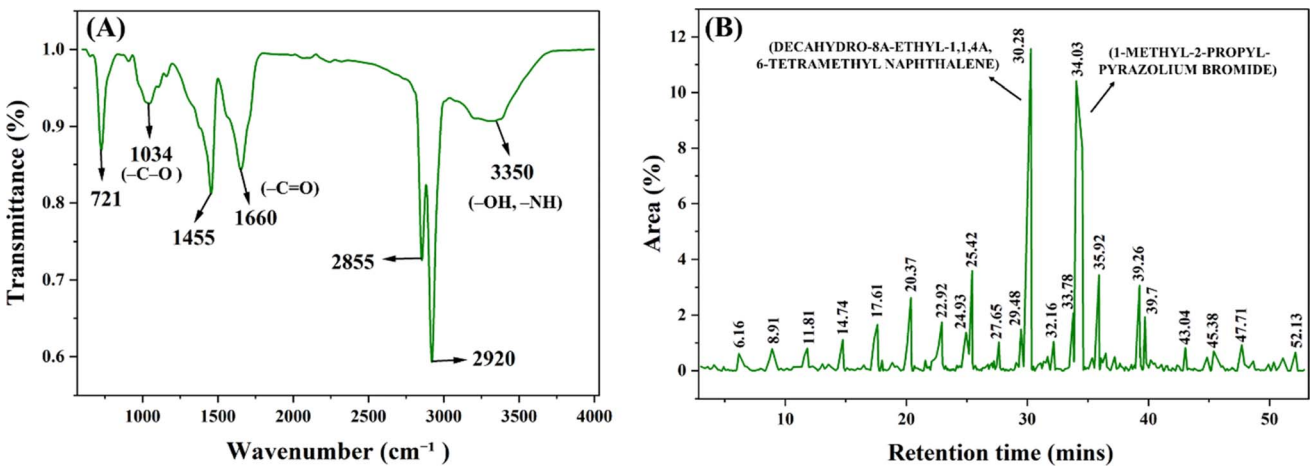

Fig. 6 (A) FTIR spectra highlighting functional groups present in biofuel derived from FW pyrolysis; (B) GC-MS chromatograms indicating distinct organic compounds in the resulting biofuel.

Table 5 Comparative analysis of fuel properties between the studied biofuel and pyrolysis-derived biofuels from different feedstocks

Fuel properties	Studied biofuel	Switch grass[58]	Wood[59]	Palm shell[60]	Animal fat (poultry)[57]	ASTM burner fuel standard[61]
Calorific value (MJ kg^{-1})	40.24	18.00	23.10	26.93	40.32	Min 15
Dynamic viscosity (cP)	1.82	—	45.00	—	—	—
Kinematic viscosity at 40 °C (cSt)	2.12	19.30	134.00	1.75	5.32	Max 125
Specific gravity	0.86	—	1.18	—	—	—
Density (kg m^{-3})	860.00	1150.00	—	1110	886.20	—
Acid value (mg KOH per g)	16.00	—	—	—	124.34	—
Flash point (°C)	60.00	—	50.00	99.00	46.00	Min 45
Fire point (°C)	78.00	—	—	—	—	—
Moisture content (%)	30.00	32.70	22.00	48.78	0.70	Max 30
Ash content (%)	0.01	0.51	>0.01%	0.07	—	Max 0.25
pH	8.50	3.24	2.50	2.98	2.90	—

The biofuel also contained trace levels of sulfur and halogen compounds, indicating that further purification or detoxification is necessary to meet strict environmental standards. Finally, the presence of low concentration silane derivatives and urea-derived compounds suggests potential for selective material recovery or niche chemical applications.

Based on the tanning process, sulfur in FW is expected to originate mainly from inorganic sulfides (*e.g.*, sodium sulfide/hydrosulfide used during unhairing) and sulfur-containing amino acids (such as cysteine and methionine) present in collagen of lime fleshing.[64] During pyrolysis, these sulfur sources might transform into various organosulfur compounds. Supporting this, GC-MS analysis of the produced biofuel identified trace sulfur-containing compounds, including thiane derivatives (*e.g.*, *trans*-2-methyl-4-*n*-pentylthiane *S*,*S*-dioxide) and sulfur pentafluoride-related species, confirming the presence and transformation of sulfur species (SI Table S3). Importantly, the ultra-low sulfur content (Table 1) suggests minimal environmental impact and reduced potential for SO_X emissions.

4. Conclusion

This study confirms the feasibility of producing biofuel from fleshing waste (FW) from the leather industry *via* pyrolysis, with optimization using response surface methodology. The pyrolysis process produced 55% biofuel at 555 °C for 60 minutes with a nitrogen flow rate of 1 L h^{-1}. The Quadratic model provided a good fit for identifying the relationships between biofuel yield and the parameters (temperature, time, and N_2 flow rate). This is confirmed by a high R^2 of 0.9823 and an adequate precision of 29.4692. The effects of temperature and time were parabolic for biofuel yield, while the N_2 flow rate showed a linear inverse correlation. Characterization of the fuel properties showed that the synthesized biofuel is suitable for direct energy use, with a calorific value of 40.24 MJ kg^{-1}, a dynamic viscosity of 1.82 cP, a kinematic viscosity of 2.12 cSt, and a density of 860 kg m^{-3}. Its better stability is reflected in an acid value of 16 mg KOH per g of fuel, and safety is indicated by flash and fire points of 60 °C and 78 °C, respectively. FTIR analysis of biofuel showed absorption bands at around 3350, 2920, 2855, 1660, and 1455 cm^{-1} associated with –OH and –NH stretching, –CH stretching, –C=O stretching, and –CH bending groups. The result is also well correlated with the detection of a range of hydrocarbons, oxygenates, and nitrogen-containing compounds by GC-MS.

The research concentrates on the advantages of mitigating waste issues in Bangladesh's leather industry for developing a sustainable waste management system aligning with SDG 7 (Affordable and clean energy), SDG 8 (Decent work and economic growth), SDG 12 (Responsible consumption and production), and SDG 13 (Climate action). In addition to biofuel, the pyrolysis of FW also generates about 40% biochar and 5% syngas under optimized conditions. Although external energy input is required for pyrolysis, the process can be optimized by utilizing pyrolysis by-products (*e.g.*, syngas or char) as internal energy sources, thereby reducing reliance on fossil-based electricity. The char has also potential for value-added applications, such as carbon sequestration, soil amendment, and environmental remediation. A comprehensive life cycle assessment (LCA) would be necessary to fully quantify the net GHG emissions from the biofuel produced. Hence, future investigations should explore LCA, characterization, and utilization of by-products to enhance overall sustainability and circularity with zero waste discharge.

Author contributions

Mohammad Al Shahriar Khan: investigation, writing – original draft, visualization, validation, formal analysis, software, Manjushree Chowdhury: writing – review & editing, validation, Masud Hassan: writing – review & editing, validation, Amal Kanti Deb: conceptualization, methodology, data curation, visualization, validation, writing – review and editing, supervision, resources.

Conflicts of interest

The authors declare that they have no affiliations with any organization or entity that could have influenced the content of this manuscript.

Data availability

On behalf of all authors, the corresponding author would like to confirm that most of the data generated in this research is presented in the article. The additional data supporting this article has been included as part of the supplementary information (SI). Supplementary information: formulas eqn (S1)–(S5) (SI text I), statistical comparison of regression models (Table S1), cost analysis of biofuel (Table S2), compounds identified in GC-MS analysis (Table S3), purified biofuel fraction based on boiling point at 40–60 °C (Fig. S1), purified biofuel fraction based on boiling point at 60–80 °C (Fig. S2), biochar synthesized at 550 °C (Fig. S3). See DOI: https://doi.org/10.1039/d5ra10133f.

Acknowledgements

Mohammad Al Shahriar Khan extends his gratitude to the Ministry of Science and Technology, Bangladesh, for providing him with the National Science and Technology (NST) fellowship. The authors express their gratitude to the Centre for Advanced Research in Sciences (CARS) at the University of Dhaka and ILET Advanced Lab for their assistance with experimental works and instrumental analyses. The authors are especially grateful to the managment of Arafat Tannery for providing the fleshing waste samples.

References

1 D. Masilamani, B. Madhan, G. Shanmugam, S. Palanivel and B. Narayan, *J. Clean. Prod.*, 2016, **113**, 338–344.
2 K. V. Sandhya, S. Abinandan, N. Vedaraman and K. C. Velappan, *Waste Manage.*, 2016, **48**, 638–643.
3 M. Hashem, M. N. A. Tomal and B. Mondal, *Bangladesh J. Sci. Ind. Res.*, 2015, **50**, 227–232.
4 P. Puhazhselvan, A. Pandi, P. B. Sujiritha, G. S. Antony, S. N. Jaisankar, N. Ayyadurai, P. Saravanan and N. R. Kamini, *Process Saf. Environ. Prot.*, 2022, **157**, 59–67.
5 N. Uddin, T. R. Tamanna, M. Fateh, A. Khan Panni and M. I. Hossain, *Eur. J. Eng. Technol. Res.*, 2023, **8**, 31–36.
6 C. B. Agustini, F. Spier, M. da Costa and M. Gutterres, *Resour. Conserv. Recycl.*, 2018, **130**, 51–59.
7 B. Ravindran and G. Sekaran, *Waste Manage.*, 2010, **30**, 2622–2630.
8 E. Alptekin, M. Canakci and H. Sanli, *Fuel*, 2012, **95**, 214–220.
9 S. Chatterjee, A. Das, D. Paul, S. Chakraborty and P. Choudhury, *J. Environ. Manage.*, 2023, **343**, 118141.
10 S. Yaman, *Energy Convers. Manag.*, 2004, **45**, 651–671.
11 A. Al-Rumaihi, M. Shahbaz, G. Mckay, H. Mackey and T. Al-Ansari, *Renewable Sustainable Energy Rev.*, 2022, **167**, 112715.
12 K. P. Shadangi and K. Mohanty, *Fuel*, 2014, **115**, 434–442.
13 V. Chiodo, G. Zafarana, S. Maisano, S. Freni and F. Urbani, *Fuel*, 2016, **164**, 220–227.
14 S. L. Lo, Y. F. Huang, P. Te Chiueh and W. H. Kuan, in *Energy Procedia*, Elsevier Ltd, 2017, 105, 41–46.
15 K. A. Roni, Z. Mufrodi, B. Putri Irani and L. Legiso, *Int. J. Res. Innovat. Appl. Sci.*, 2025, **10**, 625–631.
16 M. Velusamy, B. Chakali, S. Ganesan, F. Tinwala and S. Shanmugham Venkatachalam, *Environ. Sci. Pollut. Res.*, 2020, **27**, 29778–29790.
17 S. A. Afolalu, O. O. Yusuf, A. A. Abioye, M. E. Emetere, S. O. Ongbali and O. D. Samuel, *IOP Conf. Ser. Earth Environ. Sci.*, 2021, **665**, 012040.
18 M. S. Karimi, S. Arif and B. Noori, *Int. J. Biol. Phys. Chem. Stud.*, 2025, **7**, 06–13.
19 S. Chakraborty, V. Aggarwal, D. Mukherjee and K. Andras, *Asia-Pac. J. Chem. Eng.*, 2012, **7**, 254–262.
20 X. Ji and X. Long, *Renewable Sustainable Energy Rev.*, 2016, **61**, 41–52.
21 T. F. Stocker, D. Qin, G.-K. Plattner, M. M. B. Tignor, S. K. Allen, J. Boschung, A. Nauels, X. Yu, V. Bex and P. M. Midgley, *Climate Change 2013: the Physical Science Basis: Summary for Policymakers, Technical Summary and Frequently Asked Questions*, Intergovernmental Panel on Climate Change, 2013, vol. 1, pp. 31–115.
22 H. Dagne, R. Karthikeyan and S. Feleke, *J. Energy*, 2019, **2019**, 7329269.
23 A. M. Yahya, A. A. Adeleke, P. Nzerem, P. P. Ikubanni, S. Ayuba, H. A. Rasheed, A. Gimba, I. Okafor, J. A. Okolie and P. Paramasivam, *ACS Omega*, 2023, **8**, 43771–43791.
24 C. C. Seah, S. H. Habib, R. S. R. M. Hafriz, A. H. Shamsuddin, N. M. Razali and A. Salmiaton, *Results Eng.*, 2024, **22**, 102301.
25 K. Akubo, M. A. Nahil and P. T. Williams, *J. Energy Inst.*, 2019, **92**, 1987–1996.
26 M. E. A. Dahou, S. Dehmani, C. Dehmani and D. Zerrouki, *Pol. J. Environ. Stud.*, 2025, **34**, 5067–5075.
27 J. A. Oyebanji, P. O. Okekunle, O. A. Lasode and S. O. Oyedepo, *Biofuels*, 2018, **9**, 479–487.
28 A. Koochzakzaei, M. S. Bidgoli and S. Safapour, *J. Am. Leather Chem. Assoc.*, 2022, **117**, 515–519.
29 G. Griyanitasari, I. F. Pahlawan and E. Kasmudjiastuti, *IOP Conf. Ser. Mater. Sci. Eng.*, 2018, **432**, 012040.
30 A. R. Akhi, A. K. Deb, M. Hassan and S. K. Paul, *ACS Omega*, 2025, **10**, 48349–48369.
31 D. Glushkov, D. Klepikov, A. Nigay, K. Paushkina and A. Pleshko, *Appl. Sci.*, 2023, **13**, 3501.
32 A. Wolak, G. Zajac and T. Słowik, *Sensors*, 2021, **21**, 2530.
33 P. A. P. Decote, L. Negris, A. P. Vidoto, L. A. N. Mendes, E. M. M. Flores, M. A. Vicente and M. F. P. Santos, *Fuel*, 2022, **313**, 122642.
34 J. M. Hughes, R. H. Dennis and E. J. Beal, *Energy Fuels*, 1996, **10**, 1276–1277.
35 D. J. Graham, B. Jaselskis and C. E. Moore, *J. Chem. Educ.*, 2013, **90**, 345–351.
36 L. R. Cavonius, N. G. Carlsson and I. Undeland, *Anal. Bioanal. Chem.*, 2014, **406**, 7313–7322.
37 A. Ganesh Kumar, S. Swarnalatha, B. Sairam and G. Sekaran, *Bioresour. Technol.*, 2008, **99**, 1939–1944.
38 M. González-Lucas, M. Peinado, J. J. Vaquero, L. Nozal, J. L. Aguirre and S. González-Egido, *Energies*, 2022, **15**, 1273.
39 A. Bahillo, L. Armesto, A. Cabanillas and J. Otero, *Trans. ASME, J. Energy Resour. Technol.*, 2006, **128**, 99–103.
40 J. Kluska, M. Ochnio, D. Kardaś and Ł. Heda, *Waste Manage.*, 2019, **88**, 248–256.

41 R. Chagtmi, A. Ben Hassen Trabelsi, A. Ben Abdallah, A. Maaoui, G. Lopez, M. Cortazar, H. Khedira, C. Chaden and M. Olazar, *Sustain. Chem. Pharm.*, 2023, **33**, 101130.
42 C. Branca, G. D'Angelo, C. Crupi, K. Khouzami, S. Rifici, G. Ruello and U. Wanderlingh, *Polymer*, 2016, **99**, 614–622.
43 M. Asemani and A. R. Rabbani, *J. Pet. Sci. Eng.*, 2020, **185**, 106618.
44 S. Ulpathakumbura, N. Marikkar, L. Jayasinghe and A. History, *Int. J. Plant Biol. Based Pharmaceut.*, 2023, **3**, 104–113.
45 T. Riaz, R. Zeeshan, F. Zarif, K. Ilyas, N. Muhammad, S. Z. Safi, A. Rahim, S. A. A. Rizvi and I. U. Rehman, *Appl. Spectrosc. Rev.*, 2018, **53**, 703–746.
46 E. Apaydın Varol and Ü. Mutlu, *Energies*, 2023, **16**, 3674.
47 M. Abdulla-Al-Mamun, N. Hossain, M. I. Hossain and R. Sultana, *Text. Leather Rev.*, 2023, **6**, 37–56.
48 O. Farobie, A. Amrullah, N. Syaftika, A. Bayu, E. Hartulistiyoso, W. Fatriasari and A. B. Dani Nandiyanto, *ACS Omega*, 2024, **9**, 16665–16675.
49 N. Rambhatla, T. F. Panicker, R. K. Mishra, S. K. Manjeshwar and A. Sharma, *Results Eng.*, 2025, **25**, 103679.
50 I. Y. Mohammed, Y. A. Abakr, F. K. Kazi, S. Yusuf, I. Alshareef and S. A. Chin, *Bioresources*, 2015, **10**, 6457–6478.
51 N. H. Elsayed, G. M. Taha and O. A. Mohamed, *J. Biomed. Res. Environ. Sci.*, 2021, **2**, 1035–1043.
52 G. C. Basak, L. Goswami, B. Chattopadhyay and A. Bandyopadhyay, *Polym. Polym. Compos.*, 2012, **20**, 279–288.
53 M. F. Ali, M. S. Hossain, S. Ahmed and A. M. Sarwaruddin Chowdhury, *Heliyon*, 2021, **7**, e06954.
54 M. F. Ali, M. A. Ahmed, M. S. Hossain, S. Ahmed and A. M. Sarwaruddin Chowdhury, *Compos., Part C: Open Access*, 2022, **9**, 100320.
55 C. Invernizzi, T. Rovetta, M. Licchelli and M. Malagodi, *Int. J. Anal. Chem.*, 2018, **2018**, 7823248.
56 A. Elena, I. Gozescu, A. Dabici, P. Sfirloaga and Z. Szabadai, *Macro to Nano Spectroscopy*, IntechOpen, London, 2012.
57 A. Ben Hassen-Trabelsi, T. Kraiem, S. Naoui and H. Belayouni, *Waste Manage.*, 2014, **34**, 210–218.
58 R. He, X. P. Ye, B. C. English and J. A. Satrio, *Bioresour. Technol.*, 2009, **100**, 5305–5311.
59 D. Vamvuka, *Int. J. Energy Res.*, 2011, **35**, 835–862.
60 P. Weerachanchai, C. Tangsathitkulchai and M. Tangsathitkulchai, *SAE Technical Papers*, 2007, DOI: 10.4271/2007-01-2024.
61 A. Oasmaa, A. Källi, C. Lindfors, D. C. Elliott, D. Springer, C. Peacocke and D. Chiaramonti, *Energy Fuels*, 2012, **26**, 3864–3873.
62 D. Pradhan, R. K. Singh, H. Bendu and R. Mund, *Energy Convers. Manag.*, 2016, **108**, 529–538.
63 S. Nanda, P. Mohanty, J. A. Kozinski and A. K. Dalai, *Energy Environ. Res.*, 2014, **4**, 21–32.
64 A. D. Covington and W. R. Wise, in *Tanning Chemistry: the Science of Leather*, The Royal Society of Chemistry, Cambridge, 2nd edn, 2019, vol. 1, pp. 05–26.